



Cite this: DOI: 10.1039/c4ce01499e

Heat-treatment of metal–organic frameworks for green energy applications

Lacey Lux,[†] Kia Williams[†] and Shengqian Ma^{*}

Increasing population, global climate change, and dwindling fossil fuel reserves have led to a green energy revolution in the past few years, particularly in the fields of green energy generation and storage. While fuel cell, lithium-ion batteries, and supercapacitors are far from technical jargon in today's world, the sheer number of these devices is not accurately exhibited in the consumer market. Metal–organic frameworks (MOFs) are an emerging class of crystalline materials consisting of metal ion nodes and organic linkers that has shown promise in the fields of gas capture, gas storage, separations, catalysis, magnetism, fluorescence, and sensing to name only a few. The use of these materials as self-sacrificing templates, *via* calcination or pyrolysis, for the design of green energy generation and storage devices is the focus of this review.

Received 19th July 2014,
Accepted 6th September 2014

DOI: 10.1039/c4ce01499e

www.rsc.org/crystengcomm

1. Introduction

With increasing population and usage of fossil fuels, the need for alternative and sustainable energy technologies has become a necessity. Not only must such technology need to, at least, match the general activity of current energy storage conversion and storage devices, but there is also a need for feasible and affordable application and distribution. Interests such as fuel cells, batteries, capacitors, solar cells, *etc.* afford much opportunity for improvement and research focus.¹ Metal–organic frameworks (MOFs) are a class of porous materials consisting metal ions or clusters coordinated by organic ligands. They are highly crystalline materials with a large structural diversity and permanent porosity. These features, along with the ability to fine tune the structure with various ligands and metal centers, lead to an array of applications including gas capture and storage,² separations,³ catalysis,⁴ magnetism applications,⁵ fluorescence and sensing applications,⁶ and more in this rapidly developing field. The facile modification, as it relates to the tunability of the crystalline pore sizes and surface areas of MOFs, affords this class of compounds a high abundance of resultant structures in comparison to other classes of porous materials. Additionally, thermally activated MOFs impart distinct advantages to these materials when compared to their parent structures including electrolytic conductivity, a higher resistance to corrosion by the electrolyte, and a uniform distribution of catalytic centers affixed to a carbon support.

MOFs have been studied for many energy related applications, particularly for gas storage and separations. What is less explored, however, is the use of MOFs as templates/precursors for energy conversion and storage devices. MOFs have shown early promise in different aspects of these technologies, and, being a relatively new field, there is still much more to be explored.⁷ In this review, we aim to narrow the focus on one very intriguing property of MOFs, the ability to serve as a template or self-sacrificing precursor for electrochemical applications after thermal treatment. This topic will cover the heat treatment of MOFs, including pyrolysis and calcination, and how it is applied in fuel cells, lithium-based batteries, and electric double-layer capacitors.

2. Fuel cells and MOFs as electrocatalyst precursors

Fuel cells comprise a widely studied group of energy conversion devices, offering efficient alternative fuel use and low emissions. According to the U.S. Department of Energy (DOE), over 200 light duty vehicles, more than 20 fuel cell buses, and approximately 60 fueling stations are currently in use in transportation applications in the U.S., and GM, Toyota, Honda, Hyundai, and other vehicle manufacturers intend to commercialize fuel cell vehicles by 2015.⁸ In order for fuel cells to be an adequate replacement for internal combustion engines (ICEs), there are key factors to be addressed and overcome. Herein, we will discuss different fuel cell types and the applications and challenges of heat-treated MOFs within them.

Several types of fuel cells, including polymer electrolyte membrane fuel cells (PEMFCs), direct ethanol fuel cells (DEFCs), and direct borohydride fuel cells (DBFCs) have been

Department of Chemistry, University of South Florida, 4202 East, Fowler Avenue, Tampa, Florida 33620, USA. E-mail: sqma@usf.edu; Fax: +1 813 974 3203; Tel: +1 813 974 5217

[†] These two authors provided equal contribution to this work.

targeted for MOF usage.^{8,9} It is widely accepted that platinum group metal (PGM) materials are the preferred catalyst at both the anode and the cathode. Despite this, the oxygen reduction reaction (ORR) at the cathode is typically significantly lower than the fuel oxidation at the anode (Fig. 1).¹⁰ Overcoming the slow kinetics requires increasing Pt content, which not only leads to higher fuel cell stack costs due to limited Pt reserves, but also lower durability, as Pt is subject to contamination.¹¹ In addition to attempting to reduce Pt loading, increasing efforts have designing non-platinum group metal (non-PGM) and metal-free catalysts to replace PGM catalysts. The DOE target for 2020 is to develop a 60% peak-efficient, direct hydrogen fuel cell with 5000 hour durability at \$30 kW⁻¹.¹²

The accessibility of metal-ion sites in MOFs, high volumetric density, and high micropore surface area give MOFs an ideal potential as catalyst precursors with no need of an additional carbon source prior to pyrolysis. To date, MOFs have been studied for use in fuel cells as both catalysts and as proton conductive membranes; however, only MOFs in use in catalyst design will be discussed in this work.

2.1 MOFs as precursors for precious metal electrocatalysts

DEFCs use ethanol as a liquid fuel source, and, thus, hold an advantage to PEMFCs in storage and transportation.¹³ They are not, however, immune to the challenges of current fuel cell technologies. Currently, platinum based catalysts are still accepted as most effective for the ethanol oxidation reaction (EOR) at the anode and ORR at the cathode. Nadeem *et al.* synthesized and studied the use of a MOF-5 (Zn₄O(bdc)₃, bdc = 1,4-benzenedicarboxylate) derived porous carbon (PC-900) as a support for PtFe nanoparticles.^{9a} MOF-5 was carbonized at 900 °C, then doped with PtFe nanoparticles resulting in PtFe/PC-900. This EOR catalyst was compared to PtFe and Pt supported by Vulcan XC72 carbon catalysts, which were deemed PtFe/XC-72 and Pt/XC-72, respectively. The calculated electrochemically active surface area (ECSA) for PtFe/PC-900 was found to be 105.32 m² g⁻¹ compared to 73.31 m² g⁻¹ for PtFe/XC-72 and 44.11 m² g⁻¹ for Pt/XC-72. This was mainly attributed to the high dispersion of PtFe nanoparticles due to the larger Brunauer–Emmett–Teller (BET) surface area of

PC-900 in comparison to XC-72. PtFe/PC-900 also shows high power density of 121 mW cm⁻² and has a normalized activity per gram of Pt of 6.8 mA g⁻¹ Pt.

Further evidence for the advantage of MOF-5 as a precursor for carbon support comes from a similar work by Yi *et al.* wherein MOF-5 was carbonized with furfuryl alcohol (FA) for use in a Pt based catalyst for DBFCs, and deemed Pt/NPC.¹⁴ DBFCs are promising energy conversion alternatives in which aqueous borohydride solutions serve as fuel. Their fast anode kinetics, high theoretical open circuit voltage (OCV), and high energy density represent only a few of the many advantages that DBFCs provide in comparison to ICEs.¹⁵ As with most fuel cell types, the high cost and limited availability of the precious metals used at catalysts debilitate the commercialization potential of DBFCs. In Yi's work, Pt/NPC was also compared to Pt supported on XC-72 (Pt/XC-72). Pt/NPC not only shows a 36.38% higher current density than Pt/XC-72 for direct borohydride oxidation, but also has a power density of 54.34 mW cm⁻² at 25 °C while Pt/XC-72 has a power density of 34.13 mW cm⁻².

PEMFCs are the most widely studied fuel cells for mobile applications, owing to the use of hydrogen as a fuel and oxygen from the air as an oxidant to produce electricity, with water as the major byproduct. Kaliaguine *et al.* introduced Pt atoms into MOF-253 (Al(OH)(bpydc), bpydc = 2,2'-bipyridine-5,5'-dicarboxylate) and pyrolyzed at temperatures ranging from 700–1050 °C, to reveal Pt nanoparticles (Pt-MOF) (Fig. 2).¹⁶ N₂ isotherms of Pt-MOF show a decreased BET surface area and reveal mesopores, micropores, and a decrease in pore volume. After the removal of Al species, catalytic activity was tested at both the anode and the cathode for Pt-MOF treated at both 950 °C (C₃) and 1050 °C (C₄) and compared to the commercial electrode (BASF, 0.5 mg_{Pt} cm⁻²). The anode results of C₃ proved more impressive, resulting in an OCV of ~970 mV, comparable to the ~960 mV of the commercially available electrocatalyst. Furthermore, the current densities at 0.6 V Pt-MOF and the commercial catalyst are 482 mA cm⁻² and 537 mA cm⁻², respectively, while the power densities are 0.58 W mg_{Pt}⁻¹ and 0.64 W mg_{Pt}⁻¹, respectively.

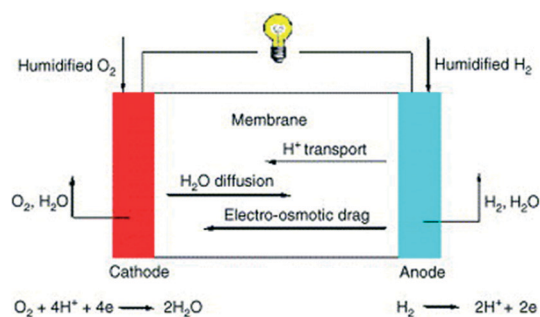


Fig. 1 General schematic of a hydrogen fuel cell. Reprinted with permission from ref. 10. Copyright 2005, Elsevier B.V.

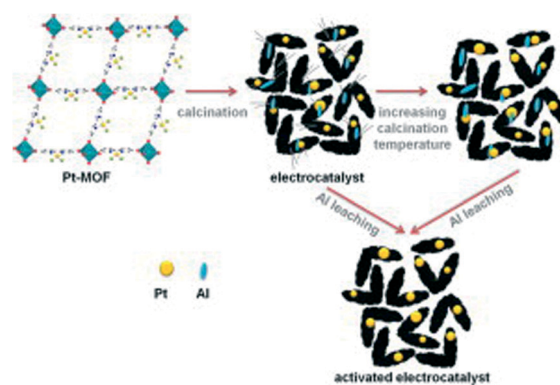


Fig. 2 Synthesis schematic of Pt-MOF from MOF-253. Reprinted with permission from ref. 16. Copyright 2013, Elsevier B.V.

2.2 MOFs as precursors for non-precious metal electrocatalysts

Previous studies have shown that macrocyclic catalysts with the Fe–N₄ moiety likely lead to a 4-electron reduction pathway of oxygen to produce H₂O as the desired product, which is one of the most important aspects of PEMFCs as clean energy sources.¹¹ Binuclear Co–N₄ moiety catalysts have also been shown to facilitate a 4-electron pathway reduction. Transition metal macrocyclic complexes generally do not have long-term stability, but thermal treatment after they have been absorbed on high surface area carbon support particles increases stability and catalytic activity.¹¹

While there are many different catalyst synthetic methods, M–N–C catalysts with metal–N_x (M–N_x, where M = Fe, Co, Ni, Mn, *etc.*) obtained through pyrolysis have shown activity in PEMFCs.^{17,18} The first example of a MOF as a precursor came in 2011 when Ma *et al.* synthesized a cobalt imidazole framework with regularly dispersed Co–N₄ moieties using Co(NO₃)₂·6H₂O and 3,5-imidazole.¹⁷ Heat treatments were done between 500–900 °C. After pyrolysis, the catalysts were treated with sulfuric acid to remove metallic cobalt. The ORR activity of the catalyst treated at 750 °C was revealed to have an onset potential of 0.83 V. The mass activity at 0.8 V and 0.75 V are 0.14 Ag⁻¹ and 1.34 Ag⁻¹, respectively. This is an increase from the mass activity of the heat-treated sample before metallic cobalt removal. In addition, an increase in surface area was observed after acid sonication. It was proposed that increase in ORR activity for the sample at 750 °C can be ascribed to the retention of high surface area and micropores, and the formation of mesopores. Rotating ring disk electrode (RRDE) measurements were taken to study the electron transfer mechanism. The Koutecky–Levich equation was employed to find the number of electrons transferred, *n*. Calculations show that 3.3–3.6 electrons were transferred during the ORR catalysis.

To date the highest peak power density catalyst for M–N₄ systems for ORR is 0.91 W cm⁻², which was first reported by Dodelet *et al.* in 2011.¹⁹ ZIF-8, a zeolitic imidazolate framework based on 2-methylimidazole, was used as a carbon support for iron(II) acetate and 1,10-phenanthroline (phen), the nitrogen source. ZIF-8, iron(II) acetate, and phen were ballmilled together in various ratios, heated at various temperatures in Ar, and then subsequently heated in NH₃. The best precursor ratio held a 20/80 mass ratio of phen to ZIF-8 and was heated at 1050 °C in Ar for 1 hour and 950 °C in NH₃. The power density at 0.6 V was found to be 0.75 W cm⁻², which is comparable to the commercial Pt catalyst. The volumetric activity of the Fe-based catalyst is increased by a factor of 2.3 in comparison to the Pt-based catalyst. This was attributed to the improved mass transport in the carbon support. This gives further evidence that the presence of both micropores and mesopores in the carbon support aid in improving activity, as Fe and N were observed to have no effect on mass transport. Since this study, many works using iron based catalysts with phen with MOF supports have been published.

Very recently, Dodelet *et al.* continued studies on this system to enhance performance and improve durability.²⁰ The catalyst previously studied was subjected to a second heat treatment in NH₃, but degrades more slowly if it only undergoes pyrolysis in Ar. Therefore, after only the initial heat treatment, the catalyst, thus named NC-Ar, was used to study activity and stability. To improve activity, the mass transport properties were targeted due to the thickness of non-PGM catalysts *versus* PGM catalysts. It was previously reported that graphitization is possible a source of stability.²¹ Adding 26 wt% carbon fibers with an average diameter of 150 nm to the catalyst precursor showed improvement in the catalyst performance; however, further heat treatments were needed to improve durability, which still remains an issue. One very important conclusion was drawn: degradation of good catalytic sites coincided with the activation of catalytic sites that were not originally active or had meager performance because of the improvement of mass transport.

ZIF-8 impregnated with furfuryl alcohol (FA) was both pyrolyzed, then doped with iron(II) acetate and phen, and doped with iron(II) acetate and phen, then pyrolyzed in Jaouen *et al.*'s recent work.²² The higher power performances observed in this work belong to those catalysts that contain not only micropores, but mesopores in the 2–4 nm range, related to the 1.8–2 nm range reported by Liu *et al.*, again providing evidence that micropore and mesopore presence in a carbon support increases mass transport properties. Moreover, it is believed that, in this case, heat treatment in heat treatment in NH₃ does not necessarily contribute to N content, but has a major function in creating micropores and small mesopores that connect already existing active sites to the surface.

In another work by Banerjee, Kurungot *et al.*, to tune porosity of the carbon materials, Zn-based multi-ligand ZIFs using imidazole/2-nitroimidazole (ZIF-70), 2-nitroimidazole/benzimidazole (ZIF-68), and 2-nitroimidazole/5-chlorobenzimidazole (ZIF-69) were embedded with iron phenanthroline complexes, [Fe(phen)₃]²⁺, and heated at 900 °C in Ar (Fig. 3).²³ It was found that the catalyst prepared from ZIF-70 (FeNC-70) has a larger surface area and is more porous, allowing for higher loading of [Fe(phen)₃]²⁺. Rotating disk electrode (RDE) measurements reveal an onset potential of 0.80 V for FeNC-70, and RRDE results show *n* values of 3.3–3.8, favoring water production.

Jaouen and coworkers also investigated the replacement of phen with 2,4,6-tris(2-pyridyl)-s-triazine (TPTZ) in the Fe^{II}/ligand/ZIF-8 precursor.²⁴ The aim was to improve previous use of TPTZ on a high surface area carbon support by Zhang *et al.* by studying Fe-ligand coordination strength.^{25,26} It was found that it is imperative that Fe remain coordinated to the ligand during the impregnation of ZIF-8 so that the Fe-ligand complex remains on the surface of the ZIF-8 particles, ensuring catalytic activity.

Liu and coworkers' work continued with another replacement of phen on a ZIF-8 support.¹⁸ An iron imidazolate framework [Fe₃(imid)₆(imidH)₂]_x, coined, FeIM, was synthesized

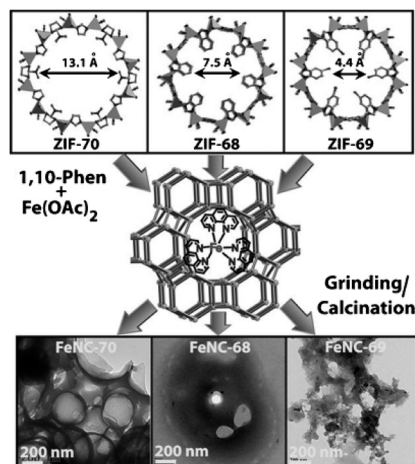


Fig. 3 Synthetic pathway of FeNC-70, FeNC-68, and FeNC-69 from $[\text{Fe}(\text{phen})_3]^{2+}$ embedded ZIF-70, ZIF-68, and ZIF-69, respectively. Reprinted with permission from ref. 23. Copyright 2013, Wiley-VCH Verlag GmbH & Co. KGaA, Weinheim.

with ferrocene and imidazole. Metallic iron was removed after heat treatment at 700, 800, and 900 °C in Ar, yielding FeIM700, FeIM800, and FeIM900, respectively. FeIM was also ballmilled with ZIF-8 and pyrolyzed at 1050 °C in Ar, then 950 °C in NH_3 for 15 minutes, giving FeIM/ZIF-8. RRDE measurements showed that FeIM700 has an onset potential of 0.855 V and n values within the range of 3.70–3.81. FeIM/ZIF-8 showed the best activity overall with an onset potential of 0.915 V. Values of n lie within the range of 3.83–3.93, highly favoring the 4-electron transfer mechanism with a H_2O_2 yield <8.6%. In this case, it is believed that the ammonia treatment increases N content. For FeIM700, FeIM800, and FeIM900, activity decreases with decreasing N content, helping support importance of N content in ORR activity.

2.3 MOFs as precursors for metal-free electrocatalysts

High surface area carbons have been targets of studies for use in various energy related applications.²⁷ Given that MOFs have already been used as precursors for high surface area carbon supports with metals, it is no surprise that they would be investigated for use with heteroatoms for applications such as fuel cells, lithium ion batteries, solar cells, *etc.* Kurungot *et al.*, utilized *in situ* graphitic carbon nitride ($g\text{-C}_3\text{N}_4$) polymerization by (a) grinding MOF-5 and melamine together before heat treatment, and (b) soaking MOF-5 and melamine in an ethanol solution prior to heat treatment (Fig. 4).²⁸ It is to be noted, unlike the ORR activities tested in the previous examples, which are typically done under acidic conditions (HClO_4 or H_2SO_4), this example and the next are under alkaline conditions. MOFCN900, the catalyst prepared under the first synthetic method and heated at 900 °C shows the highest catalytic activity of all of the samples tested, and has a current density of 4.2 mA cm^{-2} with n value of 3.12.

In order to utilize an alternative green carbon precursor in comparison to previously used FA, Cao *et al.* (a) soaked ZIF-7

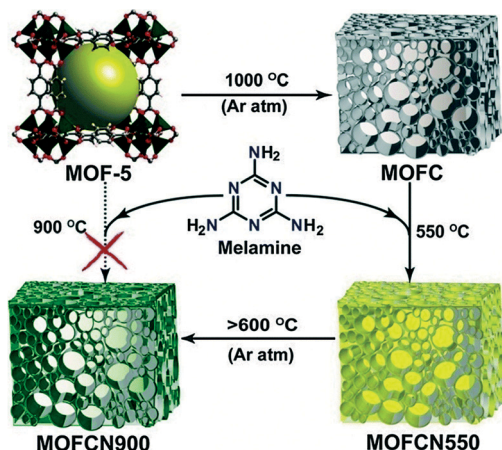


Fig. 4 Construction of MOF-derived carbon *via in situ* $g\text{-C}_3\text{N}_4$ polymerization. Reprinted with permission from ref. 28. Copyright 2014, The Royal Society of Chemistry.

($\text{Zn}(\text{NO}_3)_2 \cdot (\text{H}_2\text{O})_3$) in an aqueous glucose solution prior to pyrolysis, and (b) ground ZIF-7 and glucose together prior to pyrolysis. The results were deemed carbon-L, for the method 'a' and carbon-S for method 'b'.²⁹ Carbon-L shows an onset potential of 0.85 V vs. RHE, and with n value 3.68 at 0.3 V, close to the commercial 20% Pt/C. It was also found to be tolerant to methanol whilst the Pt/C catalyst was poisoned. Studying the chronoamperometric response in 25 000 s, carbon-L retained 75% of its relative current while 20% Pt/C only retained 53%.

2.4 Conclusions

The use of MOFs as self-sacrificing precursors for fuel cell electrocatalysts is an exceptionally fresh area of research. The first example was in 2011, and most of the works discussed in this section were published between 2013 and 2014. While strides have been made in recognizing design features of beneficial use, and some aspects of catalysts' activities have been akin to Pt based catalysts in similar conditions, major pitfalls arise in the durability of non-PGM catalysts based on MOFs. Also, although certain functionalities have been proven to have good catalytic activity, there is still a lack in understanding of the mechanisms in which ORR occurs in these catalysts, which necessitates further exploration in order to make the most efficient catalyst design.

3. Green energy storage devices and MOFs as precursors to novel electrode materials

The current global energy consumption is predicted to double within the next few decades causing an increase in global air pollution and global warming. To ameliorate the resultant negative environmental impact, there has been an increased demand for the development of green energy resources. As a result of this and in conjunction with dwindling fossil fuel

resources, there has been a considerable investigation into both green energy generation and storage systems. Devices that provide such energy storage include rechargeable batteries based on lithium ions or lithium–sulfur complexes along with electric double-layer capacitors or supercapacitors.

Lithium-ion batteries (LIB) are the current industrial standard for portable power sources in our ever-expanding universe of smartphones, laptop computers, and other portable electronic devices. Additionally, there is scientific inquiry into their potential uses as a partial power source for electric vehicles in conjunction with primary renewable energy-based fuel cells. These batteries have a number of distinct advantages for the storage of green energy including a high energy density and relatively long life span.³⁰ Batteries are the most recognizable of the green energy storage devices due to their deep integration into our everyday lives. The predominant anodic material used in today's LIBs is graphite with a theoretical capacity of 372 mA h g⁻¹.³¹ As our society has progressed further into the information age, the electronic devices that we have come to depend upon are becoming more and more energetically demanding with future devices requiring a far greater capacity than even the highest theoretical value that graphite can provide. The current push in the development of new LIBs is to develop anodes that can outperform today's graphite standard.³² Metal oxides have long been investigated for this role as they have a propensity to adopt a number of structural geometries.³³ As structural geometries necessarily impact the function of a material by tuning its chemical, physical, and electronic properties, metal oxides have the potential to provide a wide array of characteristics allowing for the optimization of energy storage in next-generation LIBs.

LIBs conventionally use a lithium metal oxide for the cathode and graphite as the anode. During charging cycles, electrons move from the cathode to the anode with the concomitant migration and intercalation of lithium ions from the cathode into the graphite anode.³⁴ During the discharge cycle, an electric current is generated by the return of the lithium cations and subsequently, the electrons to the cathode and the recombination of the electrons with the lithium ions batteries (LSB) function *via* a similar mechanism but have a higher theoretical capacity due to sulfur's large specific capacity of 1675 mA h g⁻¹.³⁵

Supercapacitors (SCs) are another fundamental source of green energy storage. Rather than the electrochemical storage that occurs in batteries, electric double-layer capacitors store energy by predominantly storing charge electrostatically in a Helmholtz layer. Moreover, pseudocapacitors store charge by both electrostatic and electrochemical energy storage methods.³⁶ Carbon electrodes, such as those used by the majority of SCs today, leave much to be desired. They often result in devices with a strong electric double-layer capacity but highly inhibited Faradaic charge storage.³⁷ Ideally, both should be incorporated into a single device to optimize its theoretical energy storage capacitance. Advantages of SCs include a very high power density, rapid charge dispersion

and response time, and exceptionally long cycling lives in comparison to the battery counterparts.³⁸ However, they are handicapped by their low energy density. Pseudocapacitors allow for the realization of a higher energy density for devices by integrating both the electric double-layer and Faradaic charge storage where oxidation/reduction reactions that take place at the surface of the electrode result in chemical energy storage analogous to the mechanism of function for a battery.³⁹

It is important to note that SCs vary fundamentally from their parent devices, capacitors.³⁷ Traditional capacitors result in the transfer of energy by charge carriers migrating between electrodes. This movement of charge results in a charge separation between the electrodes and the necessary formation of a potential between the electrodes that can be extricated and harvested *via* the application of an external circuit. On the other hand, SCs necessarily store their energy as a charge distribution in a Helmholtz double layer that interfaces with the electrolyte rather than as an electrochemical reaction. The energy density of these devices has been experimentally modulated by an increase in the electrode surface area to provide a drastic increase in the contacts that form the interface between the electrolyte and the electrode.⁴⁰ Often time, nanoporous carbonaceous materials, such as activated carbons, are used to facilitate this increase in surface area.

One facet that both batteries and SCs share is that the surface area of their electrodes is crucial for the optimization of their functionality. For commercial alkaline batteries, metallic zinc comprising part of the anode is of a powdered morphology due to its increased surface area.⁴¹ The larger surface area facilitates increased specific interaction between the electrolyte and the electrode resulting in a lowering of the internal resistance and an increase in the power density of the battery. Superconductors benefit from an increase in electrode surface area for an analogous rationale.

3.1 MOFs as precursors to lithium-based secondary batteries

A wide variety of materials have been examined for their potential application in the development of electrode materials for secondary, or rechargeable, LIBs including transition metal chalcogenides and transition metal oxides.⁴² As transition metal chalcogenides suffer from a low aggregate operating voltage against metallic lithium of *ca.* 2 V,⁴³ transition metal oxides have become a focus of the scientific community in the development of novel electrodes.⁴⁴ The investigations of these oxides are necessarily biased toward the 3d transition metals as a result of their smaller mass and dimension leading to larger electric capacities in relation to their 4d and 5d counterparts.⁴⁵

Nanometric Co₃O₄ along with other nanoscale transition metal oxides of the formula MO (M = Co, Ni, Cu, Fe) has been established as an electrode material for LIBs since the publication of a letter in *Nature* by Poizot, *et al.* in 2000.⁴⁶ Conventional synthetic strategies of nanometric Co₃O₄

preferentially result in the production of characteristic singular nanoparticles with a uniform size distribution, a trend that is ascribed to traditional homogeneous reaction conditions. Other morphologies of Co_3O_4 have also been produced including mesoporous single crystal nanoneedles⁴⁷ comprised of nanocrystal building blocks and nanowires constructed *via* a virus biotemplating synthetic methodology.⁴⁸ In comparison to the single crystal nanoparticles, both of these extended morphologies have proven to possess enhanced electrochemical performance in relation to specific capacitance, rate capability, and cycleability.

The first report of a material designed as a LIB electrode *via* a MOF-templating scheme was agglomerated Co_3O_4 by Liu, *et al.* in 2008.⁴⁹ Cobalt-MOF, $\text{Co}_3(\text{NDC})_3(\text{DMF})_4$ (NDC = 2,6-naphthalenedicarboxylate; DMF = *N,N'*-dimethylformamide) was synthesized by the solvothermal reaction of hexahydrate $\text{Co}(\text{NO}_3)_2$ and H_2NDC in DMF resolving purple crystals. Calcination of the cobalt-MOF at 600 °C resulted in the formation of the agglomerated Co_3O_4 nanoparticles. The synthesis scheme is depicted in Fig. 5, where the cobalt metal nodes of the framework are converted to metal oxide subunits and further transformed into primary nanoparticles (*ca.* 25 nm). The primary nanoparticles subsequently aggregated into a densely packed secondary nanoparticulate structure (*ca.* 250 nm; BET surface area = $5.3 \text{ m}^2 \text{ g}^{-1}$). A standard Co_3O_4 coin half-cell was constructed to determine the electrochemical capabilities of the as-prepared agglomerates at a current density of 50 mA g^{-1} . The first discharge exhibited a high discharge capacity of 1118 mA h g^{-1} and capacity retention was *ca.* 75% for the first cycle. The capacity retention reached a maximum of 965 mA h g^{-1} (86% of initial capacity) after 50 cycles. The resultant high capacity of the as-prepared Co_3O_4 agglomerate is attributed to its porous primary–secondary structural organization that provides a greater global electrode accessibility facilitating increased efficiency in electrolyte transportation and lithium-ion diffusion. The porous structure also serves to minimize the structural damage caused by lithium ion intercalation and release.

These phenomena can be confirmed within other porous morphologies of Co_3O_4 such as nanowires. Porous Co_3O_4 nanowires have been synthesized from porous coordination polymers (PCPs).⁵⁰ Hydrothermal synthesis of cobalt and nitrilotriacetic acid (NA) forms a Co–NA nanowire template.

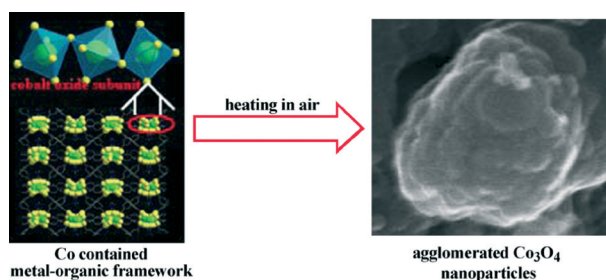


Fig. 5 Synthetic scheme for the production of agglomerated Co_3O_4 nanoparticles *via* calcination of a MOF carbon source. Reprinted with permission from ref. 49. Copyright 2010, Elsevier B.V.

Calcination of the template material at 450 °C facilitates the oxidation of cobalt and the concomitant decomposition of the template giving porous Co_3O_4 nanowires. Scanning electron microscopy (SEM) and transmission electron microscopy (TEM) determined an average nanowire length on an order of magnitude of 10 s of nm and a uniform diameter of 150 nm. The as-prepared nanowires were found to have a BET surface area of *ca.* $26 \text{ m}^2 \text{ g}^{-1}$ by N_2 sorption isotherms. Electrochemical characterization of the as-prepared Co_3O_4 nanowires proceeded by the usage of the as-prepared nanowires as the positive electrode of a standard Co_3O_4 half-cell. After the first discharge, the cathodic potential peak shows a marked decrease in the second discharge but an approximate stable discharge in cycles 2 through 10. Cyclic voltammetry experiments confirmed the initial capacity of the Co_3O_4 nanowires as 1366 mA h g^{-1} at a current density of 300 mA g^{-1} and the retention of a reversible capacity of 810 mA h g^{-1} at 30 cycles, or *ca.* 56% of its initial capacity. Synthetic reaction conditions were also investigated for significant electrochemical effect. Solvent and metal counterion composition were found to effect the nanowire morphology with homogeneous nanowire diameters resulting from water-rich phases and regular, smooth nanowires when chloride ions (Cl^-) were included as a counterion to the cobalt. The effect of Cl^- in a synthetic route employing CoCl_2 as the metallic reagent was ascribed to its hydrogen bond stabilization of the nanowires in a water-rich local environment. The decrease in the electrochemical performance from the agglomerated Co_3O_4 nanoparticles to that of the weaker as-prepared nanowire morphology is consistent with materials having higher BET surface areas resulting in decreased electrochemical performance.

Another transition metal oxide that has been studied for use in LIB electrodes is Fe_2O_3 as it has a theoretical capacity of *ca.* 1000 mA h g^{-1} ,³³ a value far greater than the theoretical capacity of conventional anodic graphite. However, it is well-known that nanometric Fe_2O_3 suffers from poor cycleability due to large volume changes upon lithium ion insertion and extraction.⁵¹ Fe_2O_3 is also known to have a low conductivity with respect to other transition metal oxides consistent with hindrance of electrochemical performance, particularly during the charge/discharge process at high current densities.⁵² Conventional methodologies have focused on altering the size and morphology of Fe_2O_3 structures *via* traditional synthetic methods. However, such techniques have produced limited candidates of which many are further impeded by production costs and sub-optimal specific capacities and rate capability.⁵³ MOF-templating has been used as an alternate method for producing spindle-like mesoporous $\alpha\text{-Fe}_2\text{O}_3$ *via* the solvothermal synthesis of MIL-88(Fe) subsequently followed by a two-step calcination process conducted at 500 °C and 380 °C sequentially.⁵¹ The former temperature under an inert atmosphere produces the $\text{FeO}_x\text{-C}$ composite; the latter under ambient gases facilitates the removal of carbonaceous residues and the formation of $\alpha\text{-Fe}_2\text{O}_3$ with a spindle-like morphology with a BET surface area of

$75 \text{ m}^2 \text{ g}^{-1}$. The synthesis scheme is shown in Fig. 6. While such a high surface area could be considered to be a detriment in some electrode materials, the surface of the as-prepared $\alpha\text{-Fe}_2\text{O}_3$ is considered to be beneficial to the two-step calcination due to the carbon formed during the first step. The formed carbonaceous residue transiently buffers the interior of the material against further structural contraction during the final heat treatment of the calcination process. The electrochemical performance of the spindle-like $\alpha\text{-Fe}_2\text{O}_3$ was considered and found to be an improvement over other $\alpha\text{-Fe}_2\text{O}_3$ morphologies. The as-prepared sample presented a Coulombic efficiency of 69% at a current density of 200 mA g^{-1} (0.2 C) after one cycle by retained a high capacity of *ca.* 97% (911 mA h g^{-1} ; discharge rate fixed at 0.1 C) from cycles 3–100 at a current density of 100 mA h g^{-1} . The relatively poor efficiency associated with the higher current density is common amongst $\alpha\text{-Fe}_2\text{O}_3$ morphologies and is attributed to the formation of a solid electrolyte interface and electrolyte decomposition causing irreversible capacity loss. The high specific capacity is attributed to its porous structure and small nanometric particles that allow for electrolyte migration and lithium-ion diffusion while remaining a buffer against volume changes inherent in lithium-ion intercalation and extraction, analogous to the rationale of the Co_3O_4 agglomerated nanoparticles. Other MOF-templated morphologies of $\alpha\text{-Fe}_2\text{O}_3$ have been produced including a nanocube structure based on MOF-templated Prussian blue nanocubes,⁵⁴ although the electrochemical properties of the agglomerated nanoparticles outweigh those of the nanocube morphology in respect to novel electrode design. Other oxides, such as cuprous and cupric, have also been used in the development

of anodic materials for LIBs as metal deficient p-type semiconductor materials although they have been outshone by other materials developed in the field.⁵⁵

LSBs have an advantage over their LIB counterparts due to their higher energy density and reduced cost.⁵⁶ Importantly, LSBs have a very high theoretical energy density of 2500 Wh kg^{-1} , which is significantly higher than the 500 Wh kg^{-1} associated with traditional LIBs.⁵⁷ Inhibitory constraints to the practical application of LSBs stem from the solubility of polysulfides in organic electrolytes and the formation of intermediates (formula: Li_2S_x ($1 \leq x \leq 8$)) during both the charging and discharging processes.⁵⁸

The high solubility of the polysulfides results in a dynamic loss of mass in the sulfur cathode leading to a drastic reduction in capacitance upon recycling. The polysulfides can also migrate through the electrolyte to the metallic lithium anode causing the formation of Li_2S , an insoluble that can result in a further decrease of long term function.⁵⁹

Examples of LSBs derived *via* the calcination or carbonization of MOF precursors include microporous carbon polyhedron (MPCPs),⁶⁰ but their performance is still unsuitable as a viable competitor of LIBs.

3.2 MOFs as precursors to novel supercapacitor electrode materials

SC electrolytes can be delineated into aqueous or organic moieties. Aqueous electrolytes, most commonly based on sulfuric acid (H_2SO_4) or potassium hydroxide (KOH), offer low internal resistance but are necessarily limited to a comparatively low operational voltage of *ca.* one volt per cell.⁶¹ Organic electrolytes, such as those based on acetonitrile or propylene carbonate (PC), allow for a higher cellular voltage due to the cost of increased internal resistance.

Liu, *et al.* produced the first MOF-templated material formulated for use in superconductors in 2008. Furfuryl alcohol (FA) was introduced into a sample of MOF-5 *via* vapor deposition resulting in the polymerization of FA within the pores of the MOF-5 framework (FA@MOF-5) upon heat treatment.⁴⁹ Pyrolysis of FA@MOF-5 at multiple temperatures resulted in distinct structures with variable surface areas. When pyrolysis was conducted at $1000 \text{ }^\circ\text{C}$, the BET surface area reached a maximum among their samples of $2872 \text{ m}^2 \text{ g}^{-1}$. At this temperature, pyrolysis of the FA@MOF-5 resulted in global framework collapse where the framework acted as a self-sacrificial scaffold for the formation of a nanoporous carbon structure. The resultant nanoporous carbon was examined as a potential novel material for superconductor electrodes in a $1.0 \text{ M H}_2\text{SO}_4$ electrolyte.

Cyclic voltammetry experiments gave a value for the capacitance of 204 F g^{-1} when considered at a sweep rate of 5 mV s^{-1} . The specific capacitance of the material was found to be as high as 258 F g^{-1} *via* galvanostatic charge/discharge experiments.

To the best of our knowledge, MOF-templated electrode materials targeted for SC using aqueous electrolytes have far

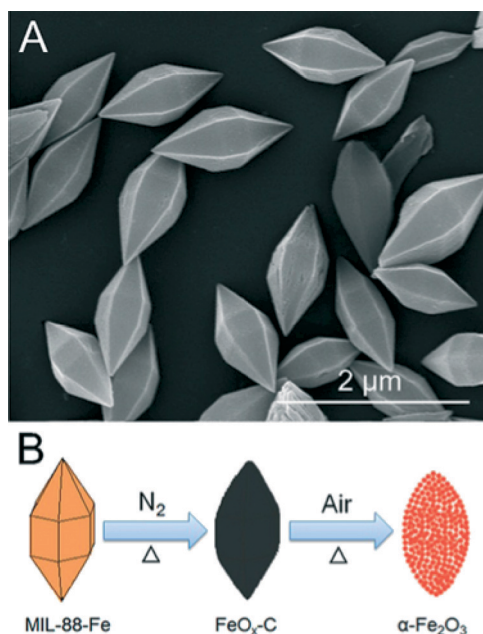


Fig. 6 (a) SEM images of the as-prepared MIL-88(Fe) (b) Synthetic scheme for the production of the spindle-like $\alpha\text{-Fe}_2\text{O}_3$ morphology *via* the calcination of a MOF carbon source.⁵⁵ Reprinted with permission from ref. 51. Copyright 2012, American Chemical Society.

out performed their organic-based counterparts. The preeminent examples of the electric double-layer capacitor anodic material produced from a MOF-templating procedure is HCPs-0.2, also denoted as a worm-like mesoporous carbon (WMC) in a previous publication.⁶⁶

Deng, *et al.* first synthesized a series of hierarchical porous carbons in 2010 from a rationally designed nonporous MOF, or a metal-organic coordination polymer (MOCP) as it is referred to in the *Materials Letters* publication.⁷² The template for the HCPs series later resulted from a synthetic deviation from the conventional MOF-5 protocol.⁶⁶ Reaction of terephthalic acid, zinc nitrate hexahydrate, and bismuth nitrate pentahydrate in DMF resulted in a crystalline product. The particular synthesis of HCPs-0.2 required 0.2 mmol of the bismuth salt. After drying and the addition of glycerol as a carbon source, the product was pyrolyzed at 1000 °C for 8 h. In total, there were four derivatives of the parent hierarchical porous carbon produced labeled by the concentration of bismuth added for each particular trial, 0, 0.1, 0.2, and 0.4 mmol of bismuth in the precursor, respectively. The electrochemical parameters of the HCPs were examined *via* galvanostatic charge/discharge experiments. For the particular example of HCPs-0.2, a combination of the HCPs-0.2 product, carbon black, and polytetrafluoroethylene (PTFE, 5%) was used as a working electrode in a conventional three-electrode experimental setup with 6 M KOH as the electrolyte. The counter and reference electrodes were nickel foil and Hg/HgO, respectively. Routine characterization confirmed a mesoporous carbon prior to calcination with pore sizes centered on 2.6 and 6.3 nm and a BET surface area of 2587 m² g⁻¹. The resultant morphology was not one of nanoparticles or nanowires, but of structures denoted as a “flower-like” structure consisting of nanosheets. The large gaps left by the aggregation of these sheets facilitates a faster transport of electrolytes through the system in comparison with traditional electrode materials or materials with a lower porosity. Galvanostatic charge/discharge experiments confirmed the functionality of the resultant product as a novel electrode material for electric double-layer capacitors with a capacitance of 344 F g⁻¹. The deviation in the synthetic route between the second paper where the resultant structure was denoted as HCPs-0.2 and the first in which it was denoted as WMC is slight. The only differing experimental parameter was the calcination temperature at 950 °C and 1000 °C, respectively. However, since the eutectic zinc-bismuth alloy produced during the synthesis of the HCPs vaporizes above 950 °C, the pertinent experimental details can be considered to be equivalent.

To the best of our knowledge, WMC/HCPs-0.2 is the best performing novel material synthesized from a MOF template or precursor for the application of SC electrodes. The second-best material formed *via* a calcination process is activated MAC (MAC-A) with a capacitance of 274 F g⁻¹, a 70 F deviation from WMC/HCPs-0.2. A selection of SC electrode materials formed by the carbonization or calcination of MOFs can be seen in Table 1 which are delineated by activity in alkaline, acidic, and ionic/organic electrolytes, respectively.

Zhou, *et al.* prepared two mesoporous carbons *via* the simple and direct pyrolysis of magnesium citrate and barium citrate.⁶⁹ The resultant materials, MgC and BaC, were further examined for their potential electrochemical efficacy in organic electrolytes. MgC proved to be the most efficient material of the two, and of all MOF-derived materials for electrode function in ionic/organic electrolytes, with a capacitance of 180 F g⁻¹ in EMImBF₄ (1-ethyl-3-methylimidazolium tetrafluoroborate). BaC synthesized from an analogous synthetic scheme was found to have a capacitance of 171 F g⁻¹ using the same electrolyte system.

Presently, it can easily be seen that novel MOF-derived electrodes formulated for use in alkaline electrolytes, primarily KOH, are superior to those functional in acidic or organic electrolytes, *i.e.* H₂SO₄ and EMImBF₃, respectively. This can be attributed to the complete ionization of KOH in solution, in comparison to sulfuric acid and organic electrolytes which undergo only partial ionization. The ionization of H₂SO₄ is only considered to be sufficiently strong during its first dissociation process leaving H₂SO₄ as a relatively electrolyte. Organic electrolytes necessarily cannot be classified as strong electrolytes but do have their advantages in the development of electrodes for SCs due to allowing for a higher operational voltage per cell.⁷³

3.3 Conclusion

While not quite as new as the use of MOFs as self-sacrificing precursors for fuel cell electrocatalysts, the use of MOFs as precursors or templates for the development of novel electrode materials for lithium-based batteries (LIB, LSB) and SCs can still be classified recently introduced area of research. In the years since the initial publications describing MOF-derived novel electrodes for both LIBs and SCs, the field has undoubtedly made significant strides in the formulation of new devices such as LSBs. While LIBs are pervasive, the field still faces a number of challenges. Some of the most dominant of these is the need for more increased structural stability that can withstand the volume changes associated with lithium-ion intercalation and extraction over longer cycling lives,⁷⁴ and needs for improved capacity, overall increased cycling lives, the development of perfectly lithium-compatible electrolytes, and batteries made of more environmentally sustainable materials.⁷⁵ While MOFs have made an impact on the field of lithium-based batteries, it is our opinion that their use in this field is only just being explored and that the innate diversity and porosity of MOFs will continue to contribute to the development of these materials. We feel that the same sentiments can be extrapolated to the use of MOFs in the development of electrodes for SCs. Shortcomings of the published MOF-derived electrodes still remain particularly the low energetics of the current devices, *i.e.* low capacitance and low energy density. The current literature on this topic has revealed that high specific surface areas, tailored pores in terms of both size and functionality, low internal electrical resistances, increased cycling performance and

Table 1 Electrode capacitances of MOF-derived carbon materials in acidic, basic, and organic/neutral salt electrolytes. Samples are arranged in the order of decreasing specific capacitance for each electrolyte, respectively

Sample	S_{BET} ($\text{m}^2 \text{g}^{-1}$)	Capacitance (F g^{-1})	Current density (mA g^{-1})	Sweep rate (mV s^{-1})	Temperature ($^{\circ}\text{C}$)	Electrolyte
Acidic electrolytes						
NPC ⁴⁹	2872	258	250	—	1000	1.0 M H ₂ SO ₄
NPC ₆₅₀ (ref. 62)	1521	222	50	—	650	1.0 M H ₂ SO ₄
AS-ZC-800 (ref. 63)	2972	211	—	10	800	1.0 M H ₂ SO ₄
C800 (ref. 27b)	2169	188	250	—	800	1.0 M H ₂ SO ₄
A-ZC-800 (ref. 63)	1341	170	—	10	800	1.0 M H ₂ SO ₄
C1000 (ref. 27b)	3405	161	250	—	1000	1.0 M H ₂ SO ₄
S-ZC-800 (ref. 63)	1955	158	—	10	800	1.0 M H ₂ SO ₄
NPC ₅₃₀ (ref. 62)	3040	158	50	—	530	1.0 M H ₂ SO ₄
NPC ₈₀₀ (ref. 62)	1141	151	50	—	800	1.0 M H ₂ SO ₄
NPC ₁₀₀₀ (ref. 62)	2524	149	50	—	1000	1.0 M H ₂ SO ₄
NPC ₉₀₀ (ref. 62)	1647	148	50	—	900	1.0 M H ₂ SO ₄
Z-800 (ref. 64)	720	130	—	50	800	1.0 M H ₂ SO ₄
Z-900 (ref. 64)	1075	128	—	50	900	1.0 M H ₂ SO ₄
Z-1000 (ref. 64)	1110	112	—	50	1000	1.0 M H ₂ SO ₄
ZC-800 (ref. 63)	1051	104	—	10	800	1.0 M H ₂ SO ₄
Basic electrolytes						
HPCs-0.2 (ref. 65)	2587	344	50	—	1000	6 M KOH
WMC ⁶⁶	2587	344	50	—	950	6 M KOH
MAC-A ⁶⁷	2222	274	250	—	MAC activated at 700	6 M KOH
HPCs-0.4 (ref. 65)	2857	241	100	—	1000	6 M KOH
MC-A ⁶⁷	1673	222	250	—	MC activated at 700	6 M KOH
HPS-0.1 (ref. 65)	2137	215	100	—	1000	6 M KOH
MPC-A ⁶⁷	1271	187	250	—	MPC activated at 700	6 M KOH
HPCs-0 (ref. 65)	1796	185	100	—	1000	6 M KOH
C-S700 (ref. 68)	817	182	—	100	700	6 M KOH
MgC ⁶⁹	2322	173	500	—	700	30% KOH
MPC ⁶⁷	1543	170	250	—	900	6 M KOH
BaC ⁶⁹	955	169	500	—	700	30% KOH
HPC ⁶⁷	1391	166	100	—	1000	6 M KOH
C-S900 (ref. 68)	704	156	—	100	900	6 M KOH
MC ⁶⁷	1812	149	250	—	900	6 M KOH
C-C1700 (ref. 68)	311	117	—	100	700	6 M KOH
MAC ⁶⁷	384	72	250	—	900	6 M KOH
Basic electrolytes						
C-C1900 (ref. 68)	199	70	—	100	900	6 M KOH
Organic/neutral salt electrolytes						
MgC ⁶⁹	2322	180	500	—	700	EMImBF ₄
3D HPC ⁷⁰	1224	175	600	—	950	1 M NEt ₄ BF ₄ in PC
BaC ⁶⁹	955	171	500	—	700	EMImBF ₄
MAC-A ⁶⁷	2222	168	250	—	MAC activated at 700	1 M NEt ₄ BF ₄ acetonitrile
MC-A ⁶⁷	1673	126	250	—	MC activated at 700	1 M NEt ₄ BF ₄ acetonitrile
MDC-D ⁷¹	3526	Ca. 120	—	50	900	1 M NaCl
MC ⁶⁷	1812	113	250	—	900	1.5 M NEt ₄ BF ₄ acetonitrile
MPC ⁶⁷	1543	111	250	—	900	1 M NEt ₄ BF ₄ acetonitrile
MPC-A ⁶⁷	1271	110	250	—	MPC activated at 700	1 M NEt ₄ BF ₄ acetonitrile
MAC ⁶⁷	384	4	250	—	900	1 M NEt ₄ BF ₄ acetonitrile

lowered cost for development will be beneficial to the development of novel electrodes for this application. It is our belief that MOFs can be prominent contributors as potential platforms for the continuing development of electrodes as they relate to renewable energy storage devices, namely lithium-based batteries and SCs.

4. Conclusions and future perspective

Worldwide climate change and the imminent decline of nonrenewable energy sources such as fossil fuels have culminated in a global search for green energy generation and

storage alternatives. MOF-derived green energy alternatives show great promise for both energy generation, *via* FCs, and energy storage, *via* LIBs, LSBs, and SCs. However, as with all work in this emerging field, there still is room for further improvement before these devices can be effectively transplanted from the laboratory to the consumer market.

Acknowledgements

The authors acknowledge the University of South Florida for the financial support of this work. Kia Williams is funded by NSF Florida-Georgia LSAMP HRD #1139850.

References

- (a) A. Choudhury, H. Chandra and A. Arora, Application of solid oxide fuel cell technology for power generation—A review, *Renewable Sustainable Energy Rev.*, 2013, **20**, 430–442; (b) X. Zhou, J. Qiao, L. Yang and J. Zhang, A Review of Graphene-Based Nanostructural Materials for Both Catalyst Supports and Metal-Free Catalysts in PEM Fuel Cell Oxygen Reduction Reactions, *Adv. Energy Mater.*, 2014, **4**, 1301523; (c) M. Zhi, C. Xiang, J. Li, M. Li and N. Wu, Nanostructured carbon-metal oxide composite electrodes for supercapacitors: a review, *Nanoscale*, 2013, **5**(1), 72–88; (d) H. Choi, C. Nahm, J. Kim, C. Kim, S. Kang, T. Hwang and B. Park, Review paper: Toward highly efficient quantum-dot and dye-sensitized solar cells, *Curr. Appl. Phys.*, 2013, **13**, S2–S13; (e) L. Lu, X. Han, J. Li, J. Hua and M. Ouyang, A review on the key issues for lithium-ion battery management in electric vehicles, *J. Power Sources*, 2013, **226**, 272–288; (f) A. J. Heeger, 25th anniversary article: bulk heterojunction solar cells: understanding the mechanism of operation, *Adv. Mater.*, 2014, **26**(1), 10–28; (g) M. Beidaghi and Y. Gogotsi, Capacitive energy storage in micro-scale devices: recent advances in design and fabrication of micro-supercapacitors, *Energy Environ. Sci.*, 2014, **7**(3), 867.
- (a) M. P. Suh, H. J. Park, T. K. Prasad and D. W. Lim, Hydrogen storage in metal-organic frameworks, *Chem. Rev.*, 2012, **112**(2), 782–835; (b) Y. He, W. Zhou, G. Qian and B. Chen, Methane storage in metal-organic frameworks, *Chem. Soc. Rev.*, 2014, **43**, 5657–5668.
- J. R. Li, J. Sculley and H. C. Zhou, Metal-organic frameworks for separations, *Chem. Rev.*, 2012, **112**(2), 869–932.
- (a) K. Leus, Y.-Y. Liu and P. Van Der Voort, Metal-Organic Frameworks as Selective or Chiral Oxidation Catalysts, *Catal. Rev.: Sci. Eng.*, 2014, **56**(1), 1–56; (b) V. Lykourinou, Y. Chen, X. S. Wang, L. Meng, T. Hoang, L. J. Ming, R. L. Musselman and S. Ma, Immobilization of MP-11 into a mesoporous metal-organic framework, MP-11@mesoMOF: a new platform for enzymatic catalysis, *J. Am. Chem. Soc.*, 2011, **133**(27), 10382–10385.
- (a) P. Canepa, Y. Chabal and T. Thonhauser, When metal organic frameworks turn into linear magnets, *Phys. Rev. B: Condens. Matter Mater. Phys.*, 2013, **87**, 094407; (b) Q. Zhang, B. Li and L. Chen, First-principles study of microporous magnets M-MOF-74 (M = Ni, Co, Fe, Mn): the role of metal centers, *Inorg. Chem.*, 2013, **52**(16), 9356–9362.
- (a) M. J. Dong, M. Zhao, S. Ou, C. Zou and C. D. Wu, A luminescent dye@MOF platform: emission fingerprint relationships of volatile organic molecules, *Angew. Chem., Int. Ed.*, 2014, **53**(6), 1575–1579; (b) L. E. Kreno, K. Leong, O. K. Farha, M. Allendorf, R. P. Van Duyne and J. T. Hupp, Metal-organic framework materials as chemical sensors, *Chem. Rev.*, 2012, **112**(2), 1105–1125.
- (a) A. Morozan and F. Jaouen, Metal organic frameworks for electrochemical applications, *Energy Environ. Sci.*, 2012, **5**(11), 9269; (b) S.-L. Li and Q. Xu, Metal-organic frameworks as platforms for clean energy, *Energy Environ. Sci.*, 2013, **6**(6), 1656.
- Multi-Year Research, Development and Demonstration Plan, 2012.
- (a) I. A. Khan, A. Badshah, N. Haider, S. Ullah, D. H. Anjum and M. A. Nadeem, Porous carbon as electrode material indirect ethanol fuel cells (DEFs) synthesized by the direct carbonization of MOF-5, *J. Solid State Electrochem.*, 2014, **18**, 1545–1555; (b) H. Furukawa, K. E. Cordova, M. O'Keeffe and O. M. Yaghi, The chemistry and applications of metal-organic frameworks, *Science*, 2013, **341**(6149), 1230444.
- B. Wang, Recent development of non-platinum catalysts for oxygen reduction reaction, *J. Power Sources*, 2005, **152**, 1–15.
- J. Zhang, *PEM Fuel Cell Electrocatalysts and Catalyst Layers*, 2008.
- D. Papageorgopoulos, *FY 2013 Annual Progress Report, DOE Hydrogen and Fuel Cells Program*, 2013.
- (a) M. Zhiani, H. A. Gasteiger, M. Piana and S. Catanorchi, Comparative study between platinum supported on carbon and non-noble metal cathode catalyst in alkaline direct ethanol fuel cell (ADEFC), *Int. J. Hydrogen Energy*, 2011, **36**(8), 5110–5116; (b) M. Z. F. Kamarudin, S. K. Kamarudin, M. S. Masdar and W. R. W. Daud, Review: Direct ethanol fuel cells, *Int. J. Hydrogen Energy*, 2013, **38**(22), 9438–9453.
- J. Liu, H. Wang, C. Wu, Q. Zhao, X. Wang and L. Yi, Preparation and characterization of nanoporous carbon-supported platinum as anode electrocatalyst for direct borohydride fuel cell, *Int. J. Hydrogen Energy*, 2014, **39**, 6729–6736.
- J. Ma, N. A. Choudhury and Y. Sahai, A comprehensive review of direct borohydride fuel cells, *Renewable Sustainable Energy Rev.*, 2010, **14**(1), 183–199.
- F. Afsahi, H. Vinh-Thang, S. Mikhailenko and S. Kaliaguine, Electrocatalyst synthesized from metal organic frameworks, *J. Power Sources*, 2013, **239**, 415–423.
- S. Ma, G. A. Goenaga, A. V. Call and D. J. Liu, Cobalt imidazolate framework as precursor for oxygen reduction reaction electrocatalysts, *Chem. – Eur. J.*, 2011, **17**(7), 2063–2067.
- D. Zhao, J.-L. Shui, C. Chen, X. Chen, B. M. Repragle, D. Wang and D.-J. Liu, Iron imidazolate framework as precursor for electrocatalysts in polymer electrolyte membrane fuel cells, *Chem. Sci.*, 2012, **3**(11), 3200.
- E. Proietti, F. Jaouen, M. Lefevre, N. Larouche, J. Tian, J. Herranz and J. P. Dodelet, Iron-based cathode catalyst with enhanced power density in polymer electrolyte membrane fuel cells, *Nat. Commun.*, 2011, **2**, 416.
- N. Larouche, R. Chenitz, M. Lefèvre, E. Proietti and J.-P. Dodelet, Activity and stability in proton exchange membrane fuel cells of iron-based cathode catalysts synthesized with addition of carbon fibers, *Electrochim. Acta*, 2014, **115**, 170–182.
- G. Wu, K. L. More, C. M. Johnston and P. Zelenay, High-performance electrocatalysts for oxygen reduction derived from polyaniline, iron, and cobalt, *Science*, 2011, **332**(6028), 443–447.
- A. Morozan, M. T. Sougrati, V. Goellner, D. Jones, L. Stievano and F. Jaouen, Effect of Furfuryl Alcohol on Metal Organic Framework-based Fe/N/C Electrocatalysts for Polymer Electrolyte Membrane Fuel Cells, *Electrochim. Acta*, 2014, **119**, 192–205.

- 23 T. Palaniselvam, B. P. Biswal, R. Banerjee and S. Kurungot, Zeolitic imidazolate framework (ZIF)-derived, hollow-core, nitrogen-doped carbon nanostructures for oxygen-reduction reactions in PEFCs, *Chem. – Eur. J.*, 2013, **19**(28), 9335–9342.
- 24 J. Tian, A. Morozan, M. T. Sougrati, M. Lefevre, R. Chenitz, J. P. Dodelet, D. Jones and F. Jaouen, Optimized synthesis of Fe/N/C cathode catalysts for PEM fuel cells: a matter of iron-ligand coordination strength, *Angew. Chem., Int. Ed.*, 2013, **52**(27), 6867–6870.
- 25 L. Zhang, K. Lee, C. W. B. Bezerra, J. Zhang and J. Zhang, Fe loading of a carbon-supported Fe–N electrocatalyst and its effect on the oxygen reduction reaction, *Electrochim. Acta*, 2009, **54**(26), 6631–6636.
- 26 A. Velázquez-Palenzuela, L. Zhang, L. Wang, P. L. Cabot, E. Brillas, K. Tsay and J. Zhang, Fe–Nx/C electrocatalysts synthesized by pyrolysis of Fe(II)–2,3,5,6-tetra(2-pyridyl) pyrazine complex for PEM fuel cell oxygen reduction reaction, *Electrochim. Acta*, 2011, **56**(13), 4744–4752.
- 27 (a) M. Pumera, Graphene-based nanomaterials for energy storage, *Energy Environ. Sci.*, 2011, **4**(3), 668; (b) H. L. Jiang, B. Liu, Y. Q. Lan, K. Kuratani, T. Akita, H. Shioyama, F. Zong and Q. Xu, From metal-organic framework to nanoporous carbon: toward a very high surface area and hydrogen uptake, *J. Am. Chem. Soc.*, 2011, **133**(31), 11854–11857.
- 28 S. Pandiaraj, H. B. Aiyappa, R. Banerjee and S. Kurungot, Post modification of MOF derived carbon via g-C₃N₄ entrapment for an efficient metal-free oxygen reduction reaction, *Chem. Commun.*, 2014, **50**(25), 3363–3366.
- 29 P. Zhang, F. Sun, Z. Xiang, Z. Shen, J. Yun and D. Cao, ZIF-derived in situ nitrogen-doped porous carbons as efficient metal-free electrocatalysts for oxygen reduction reaction, *Energy Environ. Sci.*, 2014, **7**(1), 442.
- 30 J.-M. Tarascon and M. Armand, Issues and challenges facing rechargeable lithium batteries, *Nature*, 2001, **414**(6861), 359–367.
- 31 B. Gao, A. Kleinhammes, X. P. Tang, C. Bower, L. Fleming, Y. Wu and O. Zhou, Electrochemical intercalation of single-walled carbon nanotubes with lithium, *Chem. Phys. Lett.*, 1999, **307**(3–4), 153–157.
- 32 M. Armand and J.-M. Tarascon, Building better batteries, *Nature*, 2008, **451**(7179), 652–657.
- 33 H. B. Wu, J. S. Chen, H. H. Hng and X. W. Lou, Nanostructured metal oxide-based materials as advanced anodes for lithium-ion batteries, *Nanoscale*, 2012, **4**(8), 2526–2542.
- 34 J.-M. Tarascon and D. Guyomard, Li metal-free rechargeable batteries based on Li_{1+x}Mn₂O₄ cathodes (0 < x < 1) and carbon anodes, *J. Electrochem. Soc.*, 1991, **138**(10), 2864–2868.
- 35 R. Elazari, G. Salitra, A. Garsuch, A. Panchenko and D. Aurbach, Sulfur-impregnated activated carbon fiber cloth as a binder-free cathode for rechargeable Li–S batteries, *Adv. Mater.*, 2011, **23**(47), 5641–5644.
- 36 J. Schiffer, D. Linzen and D. U. Sauer, Heat generation in double layer capacitors, *J. Power Sources*, 2006, **160**(1), 765–772.
- 37 B. E. Conway, Transition from "supercapacitor" to "battery" behavior in electrochemical energy storage, *J. Electrochem. Soc.*, 1991, **138**(6), 1539–1548.
- 38 Y. Wang, Z. Shi, Y. Huang, Y. Ma, C. Wang, M. Chen and Y. Chen, Supercapacitor devices based on graphene materials, *J. Phys. Chem. C*, 2009, **113**(30), 13103–13107.
- 39 E. Frackowiak and F. Begiun, Carbon materials for the electrochemical storage of energy in capacitors, *Carbon*, 2001, **39**(6), 937–950.
- 40 M. D. Stoller, S. Park, Y. Zhu, J. An and R. S. Ruoff, Graphene-based ultracapacitors, *Nano Lett.*, 2008, **8**(10), 3498–3502.
- 41 A. M. Bernardes, D. C. R. Espinosa and J. A. S. Tenório, Recycling of batteries: a review of current processes and technologies, *J. Power Sources*, 2004, **130**(1–2), 291–298.
- 42 A. Morozan, B. Josselme and S. Palacin, Low-platinum and platinum-free catalysts for the oxygen reduction reaction at fuel cell cathodes, *Energy Environ. Sci.*, 2011, **4**(4), 1238.
- 43 L. Heredy and L. R. McCoy, Lithium-molten Salt Cell with Transition Metal Chalcogenide Positive Electrode, *US Pat.* 3,898,096, Aug 5, 1975, 1975.
- 44 A. Lueking and R. T. Yang, Hydrogen Spillover from a Metal Oxide Catalyst onto Carbon Nanotubes—Implications for Hydrogen Storage, *J. Catal.*, 2002, **206**(1), 165–168.
- 45 M. Dekkers, G. Rijnders and D. H. A. Blank, ZnIr[_{sub} 2] O[_{sub} 4], a p-type transparent oxide semiconductor in the class of spinel zinc-d[^{sup} 6]-transition metal oxide, *Appl. Phys. Lett.*, 2007, **90**(2), 021903.
- 46 P. Poizot, S. Laruelle, S. Grugeon, L. Dupont and J.-M. Tarascon, Nano-sized transition-metal oxides as negative-electrode materials for lithium-ion batteries, *Nature*, 2000, **407**, 496–499.
- 47 X. Y. Xue, S. Yuan, L. L. Xing, Z. H. Chen, B. He and Y. J. Chen, Porous Co₃O₄ nanoneedle arrays growing directly on copper foils and their ultrafast charging/discharging as lithium-ion battery anodes, *Chem. Commun.*, 2011, **47**(16), 4718–4720.
- 48 K. T. Nam, D. W. Kim, P. J. Yoo, C. Y. Chiang, N. Meethong, P. T. Hammond, Y. M. Chiang and A. M. Belcher, Virus-enabled synthesis and assembly of nanowires for lithium ion battery electrodes, *Science*, 2006, **312**(5775), 885–888.
- 49 B. Liu, H. Shioyama, T. Akita and Q. Xu, Metal-organic framework as a template for porous carbon synthesis, *J. Am. Chem. Soc.*, 2008, **130**, 5390–5391.
- 50 C. Li, X. Yin, L. Chen, Q. Li and T. Wang, Synthesis of cobalt ion-based coordination polymer nanowires and their conversion into porous Co₃O₄ nanowires with good lithium storage properties, *Chemistry*, 2010, **16**(17), 5215–5221.
- 51 X. Xu, R. Cao, S. Jeong and J. Cho, Spindle-like mesoporous alpha-Fe₂O₃ anode material prepared from MOF template for high-rate lithium batteries, *Nano Lett.*, 2012, **12**(9), 4988–4991.
- 52 Y. C. Lee, Y. L. Chueh, C. H. Hsieh, M. T. Chang, L. J. Chou, Z. L. Wang, Y. W. Lan, C. D. Chen, H. Kurata and S. Isoda, p-Type alpha-Fe₂O₃ nanowires and their n-type transition in a reductive ambient, *Small*, 2007, **3**(8), 1356–1361.

- 53 (a) W. Cho, Y. H. Lee, H. J. Lee and M. Oh, Systematic transformation of coordination polymer particles to hollow and non-hollow In₂O₃ with pre-defined morphology, *Chem. Commun.*, 2009(31), 4756–4758; (b) W. Cho, Y. H. Lee, H. J. Lee and M. Oh, Multi ball-in-ball hybrid metal oxides, *Adv. Mater.*, 2011, 23(15), 1720–1723; (c) W. Cho, S. Park and M. Oh, Coordination polymer nanorods of Fe-MIL-88B and their utilization for selective preparation of hematite and magnetite nanorods, *Chem. Commun.*, 2011, 47(14), 4138–4140.
- 54 L. Zhang, H. B. Wu, R. Xu and X. W. Lou, Porous Fe₂O₃ nanocubes derived from MOFs for highly reversible lithium storage, *CrystEngComm*, 2013, 15(45), 9332.
- 55 (a) J. Zhang, J. Liu, Q. Peng, X. Wang and Y. Li, Nearly monodisperse Cu₂O and CuO nanospheres: preparation and applications for sensitive gas sensors, *Chem. Mater.*, 2006, 18(4), 867–871; (b) M. Izaki, T. Shinagawa, K.-T. Mizuno, Y. Ida, M. Inaba and A. Tasaka, Electrochemically constructed p-Cu₂O/n-ZnO heterojunction diode for photovoltaic device, *J. Phys. D: Appl. Phys.*, 2007, 40(11), 3326–3329; (c) B. Skarman, D. Grandjean, R. Benfield, A. Hinz, A. Andersson and L. Wallenberg, Carbon Monoxide Oxidation on Nanostructured CuO/CeO Composite Particles Characterized by HREM, XPS, XAS, and High-Energy Diffraction, *J. Catal.*, 2002, 211(1), 119–133; (d) B. White, M. Yin, A. Hall, D. Le, S. Stolbov, T. Rahman, N. Turro and S. O'Brien, Complete CO oxidation over Cu₂O nanoparticles supported on silica gel, *Nano Lett.*, 2006, 6(9), 2095–2098; (e) X. Wang, J. A. Rodriguez, J. C. Hanson, D. Gamarra, A. Martinez-Arias and M. Fernandez-Garcia, In situ studies of the active sites for the water gas shift reaction over Cu-CeO₂ catalysts: complex interaction between metallic copper and oxygen vacancies of ceria, *J. Phys. Chem. B*, 2006, 110(1), 428–434; (f) Z. Zhong, V. Ng, J. Luo, S.-P. Teh, J. Teo and A. Gedanken, Manipulating the self-assembling process to obtain control over the morphologies of copper oxide in hydrothermal synthesis and creating pores in the oxide architecture, *Langmuir*, 2007, 23(11), 5971–5977; (g) X. Zheng, X. Zhang, X. Wang, S. Wang and S. Wu, Preparation and characterization of CuO/CeO₂ catalysts and their applications in low-temperature CO oxidation, *Appl. Catal., A*, 2005, 295(2), 142–149; (h) M.-F. Luo, Y.-P. Song, J.-Q. Lu, X.-Y. Wang and Z.-Y. Pu, Identification of CuO species in high surface area CuO-CeO₂ catalysts and their catalytic activities for CO oxidation, *J. Phys. Chem. C*, 2007, 111(34), 12686–12692; (i) P. G. Harrison, I. K. Ball, W. Azelee, W. Daniell and D. Goldfarb, Nature and surface redox properties of copper(II)-promoted cerium(IV) oxide CO-oxidation catalysts, *Chem. Mater.*, 2000, 12(12), 3715–3725.
- 56 X. Ji, K. T. Lee and L. F. Nazar, A highly ordered nanostructured carbon-sulphur cathode for lithium-sulphur batteries, *Nat. Mater.*, 2009, 8(6), 500–506.
- 57 H.-J. Ahn, K.-W. Kim, J.-H. Ahn and G. Cheruvally, *Encyclopedia of Electrochemical Power Sources*, Elsevier, 2010, vol. V, p. 155.
- 58 Z. Wang, X. Li, Y. Cui, Y. Yang, H. Pan, Z. Wang, C. Wu, B. Chen and G. Qian, A Metal–Organic Framework with Open Metal Sites for Enhanced Confinement of Sulfur and Lithium–Sulfur Battery of Long Cycling Life, *Cryst. Growth Des.*, 2013, 13(11), 5116–5120.
- 59 S.-E. Cheon, K.-S. Ko, J.-H. Cho, S.-W. Kim, E.-Y. Chin and H.-T. Kim, Rechargeable Lithium Sulfur Battery, *J. Electrochem. Soc.*, 2003, 150(6), A800.
- 60 H. B. Wu, S. Wei, L. Zhang, R. Xu, H. H. Hng and X. W. Lou, Embedding sulfur in MOF-derived microporous carbon polyhedrons for lithium-sulfur batteries, *Chemistry*, 2013, 19(33), 10804–10808.
- 61 A. Burke, Ultracapacitors: why, how, and where is the technology, *J. Power Sources*, 2000, 91(1), 37–50.
- 62 B. Liu, H. Shioyama, H. Jiang, X. Zhang and Q. Xu, Metal–organic framework (MOF) as a template for syntheses of nanoporous carbons as electrode materials for supercapacitor, *Carbon*, 2010, 48(2), 456–463.
- 63 A. J. Amali, J. K. Sun and Q. Xu, From assembled metal–organic framework nanoparticles to hierarchically porous carbon for electrochemical energy storage, *Chem. Commun.*, 2014, 50(13), 1519–1522.
- 64 W. Chaikittisilp, M. Hu, H. Wang, H. S. Huang, T. Fujita, K. C. Wu, L. C. Chen, Y. Yamauchi and K. Ariga, Nanoporous carbons through direct carbonization of a zeolitic imidazolate framework for supercapacitor electrodes, *Chem. Commun.*, 2012, 48(58), 7259–7261.
- 65 S. Mo, Z. Sun, X. Huang, W. Zou, J. Chen and D. Yuan, Synthesis, characterization and supercapacitive properties of hierarchical porous carbons, *Synth. Met.*, 2012, 162(1–2), 85–88.
- 66 D. Yuan, J. Chen, S. Tan, N. Xia and Y. Liu, Worm-like mesoporous carbon synthesized from metal–organic coordination polymers for supercapacitors, *Electrochem. Commun.*, 2009, 11(6), 1191–1194.
- 67 J. Hu, H. Wang, Q. Gao and H. Guo, Porous carbons prepared by using metal–organic framework as the precursor for supercapacitors, *Carbon*, 2010, 48(12), 3599–3606.
- 68 P. Su, L. Jiang, J. Zhao, J. Yan, C. Li and Q. Yang, Mesoporous graphitic carbon nanodisks fabricated via catalytic carbonization of coordination polymers, *Chem. Commun.*, 2012, 48(70), 8769–8771.
- 69 J. Zhou, X. Yuan, W. Xing, W.-J. Si and S.-P. Zhuo, Mesoporous carbons derived from citrates for use in electrochemical capacitors, *New Carbon Materials*, 2010, 25(5), 370–375.
- 70 S.-L. Jin, H.-G. Deng, L. Zhan, W.-M. Qiao and L.-C. Ling, Synthesis of 3D hierarchical porous carbon as electrode material for electric double layer capacitors, *New Carbon Materials*, 2012, 27(2), 87–92.
- 71 S. J. Yang, T. Kim, K. Lee, Y. S. Kim, J. Yoon and C. R. Park, Solvent evaporation mediated preparation of hierarchically porous metal organic framework-derived carbon with controllable and accessible large-scale porosity, *Carbon*, 2014, 71, 294–302.
- 72 H. Deng, S. Jin, L. Zhan, Y. Wang, S. Qiao, L. Tang, X. Liang, W. Qiao and L. Ling, Synthesis and electrochemical

- performance of a laminated hollow porous carbon, *Mater. Lett.*, 2010, **64**(10), 1187–1189.
- 73 R. Kotz and M. Carlen, Principles and applications of electrochemical capacitors, *Electrochim. Acta*, 1999, **45**(15–16), 2483–2498.
- 74 J. O. Besenhard, J. Yang and M. Winter, Will advanced lithium-alloy anodes have a chance in lithium-ion batteries?, *J. Power Sources*, 1997, **68**(1), 87–90.
- 75 M. S. Whittingham, Lithium batteries and cathode materials, *Chem. Rev.*, 2004, **104**(10), 4271–4302.